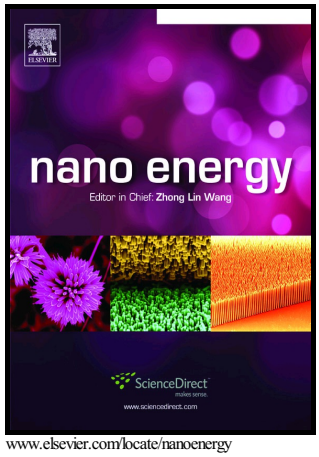

www.elsevier.com/locate/nanoenergy

Improving the reversibility of the H2-H3 phase transitions for layered Ni-rich oxide cathode towards retarded structural transition and enhanced cycle stability

Feng Wu, Na Liu, Lai Chen, Yuefeng Su, Guoqiang Tan, Liying Bao, Qiyu Zhang, Yun Lu, Jing Wang, Shi Chen, Jing Tan

PII: S2211-2855(19)30140-5
DOI: https://doi.org/10.1016/j.nanoen.2019.02.027
Reference: NANOEN3471

To appear in: *Nano Energy*

Received date: 12 December 2018
Revised date: 4 February 2019
Accepted date: 10 February 2019

Cite this article as: Feng Wu, Na Liu, Lai Chen, Yuefeng Su, Guoqiang Tan, Liying Bao, Qiyu Zhang, Yun Lu, Jing Wang, Shi Chen and Jing Tan, Improving the reversibility of the H2-H3 phase transitions for layered Ni-rich oxide cathode towards retarded structural transition and enhanced cycle stability, *Nano Energy,* https://doi.org/10.1016/j.nanoen.2019.02.027

Improving the reversibility of the H2-H3 phase transitions for layered Ni-rich oxide cathode towards retarded structural transition and enhanced cycle stability

Feng Wu[a, b, 1], Na Liu[a, b, 1], Lai Chen [*, a], Yuefeng Su[*, a, b], Guoqiang Tan[c], Liying Bao [a], Qiyu Zhang [a], Yun Lu [a], Jing Wang [a, b], Shi Chen[a, b], Jing Tan [d]

[a]School of Materials Science and Engineering, Beijing Institute of Technology, Beijing Key Laboratory of Environmental Science and Engineering, Beijing, 100081, P. R. China

[b]Collaborative Innovation Center for Electric Vehicles in Beijing, Beijing, 100081, P. R. China

[c]Chemical Sciences and Engineering Division, Argonne National Laboratory, Argonne, Illinois 60439, USA

[d]School of Chemistry and Chemical Engineering Beijing Institute of Technology Beijing, 100081, P. R. China

*Corresponding authors:

chenlai144@sina.com (L. Chen)

suyuefeng@bit.edu.cn (Y. Su)

Abstract

Although the layered Ni-rich $LiNi_xCo_yMn_{1-x-y}O_2$ ($0.7 < x < 1$, $0 < y < 0.3$) cathode materials are expected to deliver high capacity, their moderate cycle lifetime and thermal stability still hinder practical applications. There's often a tradeoff between

[1] These authors contributed equally to this work.

high capacity and structure stability since more Li^+ ions delithiated during charging will leave the structure of the layered Ni-rich materials more vulnerable. Herein, we propose that improving the reversibility of H2-H3 phase transition for Ni-rich materials is effective to tackle this challenge. It has been confirmed that the generation of microcracks and structural transformations have been suppressed since the H2-H3 phase transition becomes reversible, while which shows little effect on capacity delivery. Consequently, using Ni-rich $LiNi_{0.9}Co_{0.1}O_2$ as the cathode material, the 100^{th} capacity retention cycling at 38 mA g^{-1} has been improved remarkably from 69.7% to 97.9% by adopting this strategy. Hence, it should be a novel solution to realize both high capacity and stable cyclability for the Ni-rich cathodes.

Graphical Abstract:

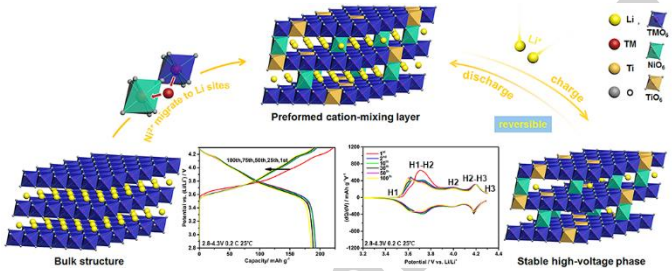

Improving the reversibility of the H2-H3 phase transitions for layered Ni-rich oxide cathode towards retarded structural transition and enhanced cycle stability

This work proposed a new way, i.e. pre-fabricating the surface of Ni-rich cathode with a cation-mixing layer through surface Ti-doping, to improve the reversibility of H2-H3 phase transition during the long cycles. The repeated formation of H3 phase in every charge-discharge process can afford the high capacity delivery, while the lossless H3 phase guarantees superior cycling stability. We consider this as a new idea to realize both high capacity and stability for Ni-rich cathodes.

Keywords:

Layered Ni-rich cathode; Surface cation-mixing layer; Third hexagonal phase; Reversibility; Phase transitions

1 Introduction

Recently, the rechargeable lithium-ion batteries (LIBs) have been widely used in portable devices, plug-in hybrid vehicles (PHEVs) and electric vehicles (EVs), due to their superior energy storage capability and environmentally friendly properties.[1-4] Layered cathode material $LiCoO_2$, the first commercialized cathode material, is now bottlenecked by the relatively low capacity in the dilemma of higher-standard requirement of energy density.[5-6] In this regard, $LiNiO_2$ has been considered as an alternative cathode due to its higher specific capacity of *ca.* 210 mAh g^{-1}.[1, 7-8]

However, the similar ion radius of Li^+ (0.076nm) and Ni^{2+} (0.069nm) enable them easy to exchange in the layered R-$\bar{3}$m structure without a dimensional mismatch.[9-10] The resulted Li/Ni cation disorder will deteriorate the electrochemistry performances of $LiNiO_2$, such as lowering the discharge capacity and accelerating the material degradation. It has been reported intensively that partial doping of Ni by other elements (Co, Mn and Al *etc.*) with optimized compositions would improve the thermal stability or cyclability in certain degrees.[11-14] Among them, Ni-rich layered oxides $LiNi_{1-x}M_xO_2$ ($0<x<0.3$) have attracted great interest owing to their significant capacity improvements, since the higher Ni content is crucial for securing a higher capacity.[15-17] Nevertheless, the higher capacity means

a more thorough delithiated state with higher concentration of thermodynamically metastable Ni^{4+} ions when charging to the certain voltage. Such highly delithiated Ni-rich oxides are expected to reduce the metastable Ni^{4+} into the more stable Ni^{2+} ions, triggering the structural transformation from layered *R*-$3\bar{m}$ to spinel *Fd*-$3\bar{m}$, and further to the rock-salt *Fm*-$3\bar{m}$.[18-19] Worse yet, the sufficient Li vacancies generated under high voltage will even accelerate such a transformation due to its kinetic nature, thus pushing forward the structure deterioration and decreasing the thermal stability.[20-24]

The formation of third hexagonal phase (H3) also occurs at high delithiated state. The phase behavior during repeated charge-discharge process of Ni-rich cathodes typically includes original hexagonal phase (H1), second hexagonal phase (H2) and third hexagonal phase (H3).[17] It has been reported that the H2 to H3 phase transition will cause an abrupt lattice contraction in the *c*-direction, leading to a large volume change and further inducing microcracks in the extended cycles.[13, 17, 25-27] Recent reports have also revealed that the capacity decay of Ni-rich cathodes is correlated with the gradual loss of H3 phase.[25] Accordingly, many efforts have been paid to improve the cyclability and thermal stability of Ni-rich cathodes by suppressing the formation of H3 phase, including introducing low-content Li_2MnO_3, lowering the Ni content, or limiting the upper cutoff voltage to 4.1 V.[17, 26-28] However, these modifications would decrease the removal of Li^+ at high voltage, *i.e.*, sacrificing the capacity at some extent to retain the stability.

To simultaneously realize high capacity and stable cyclability of Ni-rich cathode materials, the challenge is to stabilize the highly delithiated layered structure with abundant Li vacancies at high voltage. In this work, we propose that the key to deal with this challenge may lie in the reversible phase transition of H2-H3. Specifically, we achieved this goal through fabricating the Ni-rich material surface with a nanoscaled cation-mixing layer induced by surficial doping of Ti^{4+} (as shown in Scheme 1). Ni-rich $LiNi_{0.9}Co_{0.1}O_2$ as the cathode material is used here as an example to verify the validity of our strategy. It has been determined that, benefiting from improved reversibility of the H2-H3 phase transitions, the repeated formation of H3 phase in every charge-discharge process affords the high capacity delivery, meanwhile the lossless H3 phase guarantees superior cycling stability. Consequently, the modified $LiNi_{0.9}Co_{0.1}O_2$ exhibited superior cycling performance and enhanced thermal stability without expense of capacity.

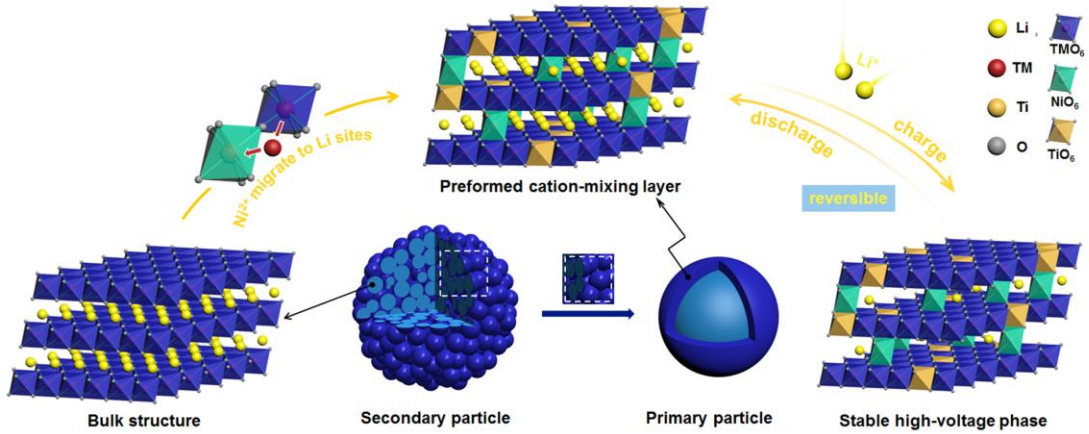

Scheme 1. Schematic view of the Ni-rich layered cathode material $LiNi_{0.9}Co_{0.1}O_2$ with a preformed cation-mixing layer at the surface.

2 Experimental section

2.1 Sample preparation

The $Ni_{0.9}Co_{0.1}(OH)_2$ precursor was synthesized via the common co-precipitation method. The starting materials $NiSO_4 \cdot 6H_2O$ and $CoSO_4 \cdot 7H_2O$ dissolved in deionized water (9:1 in molar ratio) with 0.2 mol L^{-1} total concentration was pumped into a tank reactor containing continuous stir at the bottom. At the same time, the 0.2 mol L^{-1} NaOH solution mixed with appropriate amount of $NH_3 \cdot H_2O$ was also pumped into the reactor. We set the stirring speed as 1000 rpm and kept the pH value at 11 by adjusting the pumping speed. The resulted precursors were separated by vacuum filtration, washed by deionized water and dried in a vacuum oven at 120 °C. Then, 2 g $Ni_{0.9}Co_{0.1}(OH)_2$ precursor was added into 50 mL ethanol solution (48 mL absolute ethanol and 2 mL deionized water), being stirred at room temperature. Thereafter, solutions of 0.22 mL, 0.36 mL, 0.51 mL and 0.65 mL $Ti(OC_4H_9)_4$ corresponding to the 3 mol.%-Ti, 5 mol.%-Ti, 7 mol.%-Ti and 9 mol.%-Ti respectively, were slowly dripped into the precursor solution. The mixed solution was stirred at room temperature for 4 h, and then at 45 °C for 12 h to obtain adequately hydrolyzed $Ti(OC_4H_9)_4$. During this process, the $Ti(OC_4H_9)_4$ permeated into the secondary particles and hydrolyzed to TiO_2. The products were then washed by absolute ethanol several times to clear the residual organics. After being centrifuged and dried in a vacuum oven at 80°C, the obtained products were thoroughly mixed with an appropriate amount of $LiOH \cdot H_2O$. The mixture was preheated at 450 °C for 6 h, and

then calcined at 750 °C for 12 h in the O_2 atmosphere to gain the final pristine/Ti^{4+}-doped $LiNi_{0.9}Co_{0.1}O_2$ cathode materials. The untreated material is denoted by UM, and samples with 3 mol.%, 5 mol.%, 7 mol.%, 9 mol.% Ti^{4+} doping contents are denoted by 3%-Ti PM, 5%-Ti PM, 7%-Ti PM and 9%-Ti PM.

2.2 Characterization

The crystal structure of all the samples were characterized by X-ray powder diffraction (XRD) (Rigaku UltimaIV-185 and Brucker Advance d8) with Cu Kα radiation from 2θ = 10° to 90° at a scanning rate of 0.5°·min^{-1}. In situ XRD experiments were performed with PANalytical X'Pert^3 Powder equipment. A modified coin-type half-cell with a hole at its center containing a Kapton window served as the X-ray beam path. While the cell was being charged with 40 mA g^{-1} constant current, the XRD patterns were continuously recorded every 10 min. The 2θ angles for all XRD patterns were transformed to the conventional X-ray tube Cu Kα radiation for easy comparison. The morphology of the samples was observed by a scanning electron microscopy (SEM) system (FESEM, FEI QUANTA 250) and a transmission electron microscopy (TEM) system (JEOL JEM-2100). In addition, the FIB-SEM/ Time-of-flight secondary-ion mass spectrometry (TOF-SIMS) was used to analyze the surface composition and the cross section of the samples. The Gallium ion sources based FIB-SEM and TOF-SIMS system was composed of the TESCAN LYRA instrument platform on which was mounted the TOF-SIMS analyzer. The surface chemistry states of all the samples were determined by X-ray photoelectron

spectroscopy (XPS) system (PHI QUANTERA-II SXM). The thermal stabilities of the samples were characterized by using differential scanning calorimetry (DSC, NETZSCH 200F3). For DSC test, the assembled coin-type cells were firstly charged to 4.5 V with a current of 0.2 C (38 $mA \cdot g^{-1}$) and then disassembled in the Ar-filled glovebox. DMC and DEC were used to clean the residual electrolyte on the surface of the electrodes; subsequently the electrodes were dried in the glovebox. The cathode materials were finally scraped from the electrodes and we could get about 2-5 mg powders. The powders were sealed in a high-pressure DSC sample pan with appropriate drips of electrolyte. The DSC tests were performed from 100 to 350 °C with a heating rate of 10 $°C \cdot min^{-1}$.

2.3 Electrochemical measurement

The electrochemical properties were measured by using the CR2025 coin-type cells. The electrode slurry consisted with 80 wt% of active materials, 10 wt% of carbon black, and 10 wt% poly-vinylidene fluoride (PVDF) in an N-methyl pyrrolidone (NMP) solvent, which were coated onto aluminum foil. Then the coated aluminum foil was dried at 80 °C for 48 h and pouched. The obtained cathode electrode and Li electrode were assembled into the CR2025 coin-type cells in an Ar-filled glovebox. Polypropylene (PP) film was used as a separator and 1 M $LiPF_6$ in a 1/1/1 (*v*/*v*/*v*) EC/EMC/DMC mixture was applied as electrolyte. The cells were tested at constant rate 0.2 C (1 C = 190 $mA \cdot g^{-1}$) within the potential range of 2.8-4.3 V and 2.8-4.5 V at 25 °C using a CT2001A Land instrument. We also tested the extended

electrochemical properties of the samples at 55°C. The electrochemical impedance spectroscopy (EIS) measurements were conducted on a CHI660A impedance analyzer with an AC amplitude of 5 mV over a frequency range of 100 kHz to 0.01 Hz.

3 Results and discussion

3.1 Structural changes after Ti^{4+} doping.

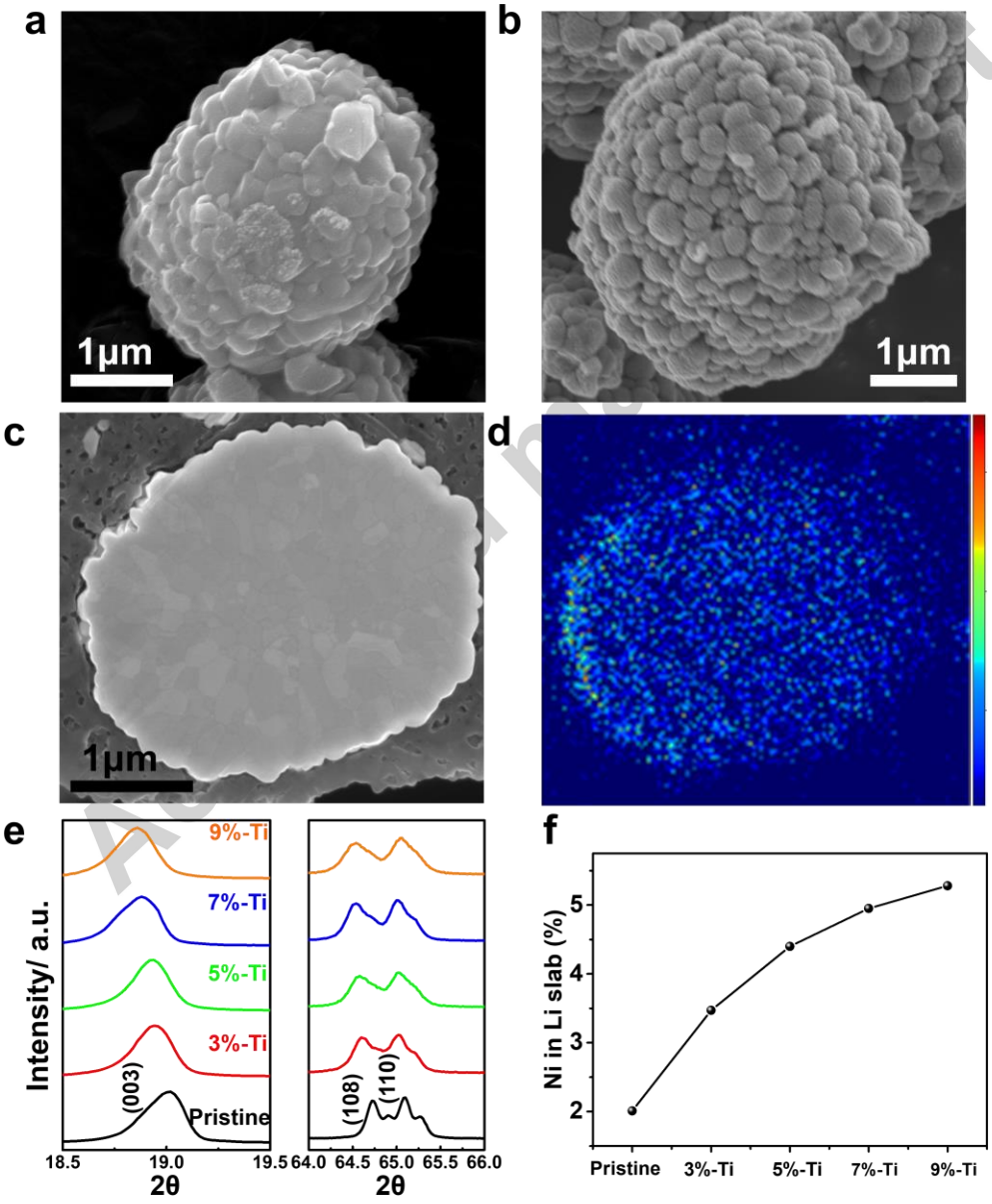

Fig. 1. SEM images of (a) UM, (b) 5%-Ti PM. (c) The cross-section SEM profile of 5%-Ti PM. (d) TOF-SIMS maps demonstrating the localization of Ti in 5%-Ti PM. (e) Local magnified XRD patterns of all the samples. (f) Occupancy of Ni^{2+} in the Li sites as a function of Ti content.

To study the effect of Ti doping on the Ni-rich cathode material, the pristine material (denoted by UM) and samples with 3 mol.%, 5 mol.%, 7 mol.%, 9 mol.% doping contents (denoted by 3%-Ti, 5%-Ti, 7%-Ti and 9%-Ti) were synthesized and investigated. The inductively coupled-plasma atomic-emission spectroscopy (ICP-AES) results shown in the Table S1 demonstrate the measured composition of the samples agree well with the target. The SEM images in Fig. 1 and Fig. S1 show that the surface of the PM samples became much rougher than the UM sample, indicating some surface reactions happened after Ti doping. TOF-SIMS cross-sectional chemical mapping (Fig. 1 c-d) and cross-section EDS mappings (Fig. S1 d-e) show the evenly distributed Ti in the particles, suggesting that Ti had permeated into the secondary particles instead of coating outside.

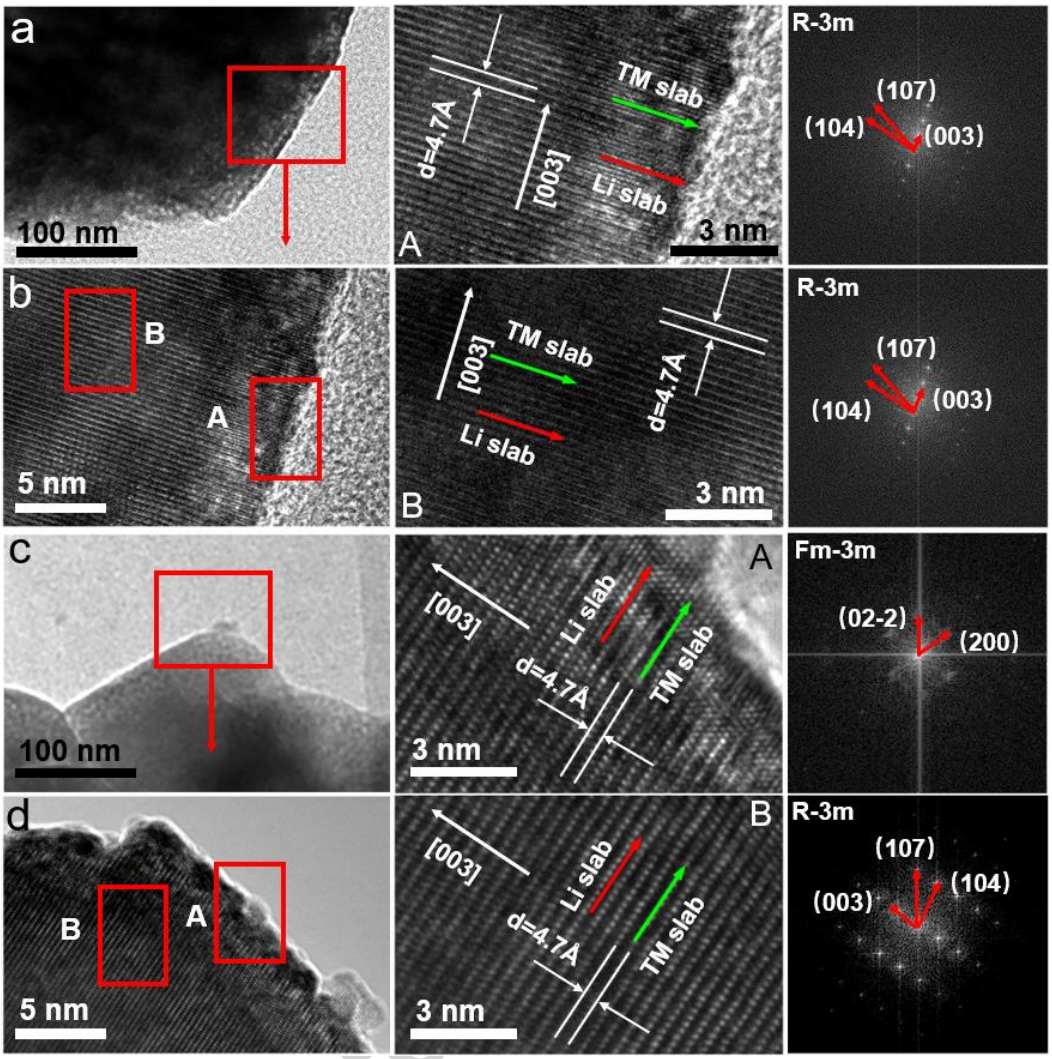

Fig. 2. TEM images of the UM (a, b) and 5%-Ti PM (c, d). The corresponding HRTEM images and FFT images of the marked rectangle regions in (b) and (d) (marked as I and II) are shown at the right of b and d, respectively.

Fig. S2 shows the XRD patterns and corresponding Rietveld refinement plots of all the samples. All of them can be characterized as hexagonal α-$NaFeO_2$ structure with *R*-$\bar{3}$*m* space group; while as shown in Fig. 1e, the (003) peaks of the PM samples show a slight shift to lower diffraction angles in accord with lager *c* values (Table S2). The expansion of interlayer spacing may result from the reduction of Ni^{3+} ions (0.060 nm) to Ni^{2+} ions with lager radius (0.069 nm) due to charge compensation from Ti^{4+}

doping.[29] It is supported by the results of XPS measurement in Fig. S3, which shows that more Ni^{2+} ions are observed at the surface after Ti^{4+} doping. In addition, Fig. S3 e shows that for each PM sample, the Ni^{2+}/Ni^{3+} ratio gets smaller with increased etched depth. Especially, there's an abrupt drop of the Ni^{2+}/Ni^{3+} ratio since the etched depth reaches 15 nm, along with the absence of signals from Ti^{4+} shown in Fig. S3 d, indicating Ti^{4+} was only doped into the surficial region and caused the reduction of surface Ni^{3+} to Ni^{2+}. However, the Ni^{2+} ions may migrate to Li layers and thus aggravating the Li/Ni cation disorder.[30] Indeed, Fig. 1f, drawn from the Rietveld refinement results (Table S2), shows increased occupancy of Ni^{2+} in the Li sites with increasing Ti^{4+} content. Accordingly, the splits of the (110)/(108) peaks of PM samples become less evident along with the gradual disappearance of edge peaks (Fig.1e), suggesting the development of less-ordered structure after Ti^{4+} doping.[31]

To confirm this less-ordered structure, TEM and HRTEM tests were applied. As shown in Fig. 2 a-b, the surface (region A) and interior (region B) regions of the UM sample both comprise orderly layered structure ($R\text{-}\bar{3}m$); that is, the Li and transition metal ions occupy in their respective slabs orderly. On contrary, in the case of the 5%-Ti PM shown in Fig. 2 c and d (images of other modified samples are shown in Fig. S4), there are transition metal ions partially occupying the Li sites, forming a mixed region with a thickness of ~5 nm. Specifically, according to the FFT images, the surface of the 5%-Ti PM shows mixed phases including NiO ($Fm\text{-}\bar{3}m$) and layered phase ($R\text{-}\bar{3}m$), while the interior region only consists of pure layered phase ($R\text{-}\bar{3}m$). Such an observation is much clearer at higher Ti content, along with the extended

mixed region from ~2 nm in the Ti-3% PM sample (Fig. S4 a-b) to ~8 nm in the Ti-9% PM sample (Fig. S4 e-f). These results are in accordance with those of XRD and XPS measurement, based on which, it is concluded that the surficial Ti^{4+} doping will induce the reduction of Ni^{3+} to Ni^{2+} at surface region, and the latter tends to migrate into Li-slabs, preforming a cation-mixing layer and causing the less-ordered structure.

3.2 Electrochemical performances.

To check the influences from the preformed cation-mixing layer, we then tested the electrochemical properties of all the samples. As shown in Fig. 3 a-c and Fig. S5 a-c, at 0.2 C (within 2.8-4.3 V, 1 C = 190 mA g^{-1}), the discharge capacity of UM sample declined rapidly from 193.9 mA h g^{-1} to 135.1 mA h g^{-1} with a 69.68% capacity retention after 100 cycles. In contrast, the cycle performance of the PM samples gradually improved with the increased Ti content. After 100 cycles, capacity retentions of 78.53%, 97.94%, 95.09% and 97.96% are attained for the 3%-Ti, 5%-Ti, 7%-Ti and 9%-Ti PM samples respectively, suggesting the bulk structure of the PM samples had been reinforced with the preformed surface cation-mixing layer. The stabilized surface structure also benefits to form stable CEI film, which also has positive effects on cycling stability.[32] However, the excessive Ti^{4+} doping seemed to influence the discharge capacity as shown in 7%-Ti and 9%-Ti PM samples (Fig. 3c). Fig. 3d compares the rate capacities of all the samples from 0.1 to 10 C rates every ten cycles, and reaches similar conclusions. When cycled at 5 C and 10 C rates,

the UM sample delivers a reversible capacity of 100.2 mA h g^{-1} and 83.4 mA h g^{-1}, while the 5%-Ti PM delivers 159.5 mA h g^{-1} and 143.4 mA h g^{-1} separately. EIS test (Fig. S6) shows that, the Rct value of 5%-Ti PM turns out much smaller than that of UM from 1st to 100th cycles, suggesting that more stable CEI film may be formed after Ti^{4+} doping. The stable CEI that may not degrade, reform or thickening would suppresses the parasitic surface reactions and benefits Li^{+} transport during the long term cycling.[33-35] Hence, the preformed cation-mixing layer with an appropriate thickness may stabilize the bulk structure as well as serve smooth transport channels for Li^{+}; on the other hand, excessive occupation of Ni^{2+} in Li slabs would hinder Li^{+} transport, though the structure becomes more robust.

We then carefully scrutinized the differential capacity *vs.* voltage profiles (dQ/dV) in Fig. 3 e-f corresponding to the charge/discharge curves in Fig. 3 a-b. As labeled in Fig. 3 e-f, there are three distinct redox oxidation peaks that can be assigned to the phase transitions from H1 to H2 and H3, respectively. [25, 31] In the case of UM, there is an obvious discharge voltage decay along with decreased oxidation/reduction peak intensities at around 4.20 V in prolonged cycling. The decrease in peak intensities indicates the gradual loss of H3 phase, which should be responsible for the faster capacity fade of UM sample.[25] While for the 5%-Ti PM, the negligible change of the peak intensities and the overlap of dQ dV^{-1} profiles within 100 cycles suggest the preformed cation-mixing layer helps improving the reversibility of H2-H3 phase transition.

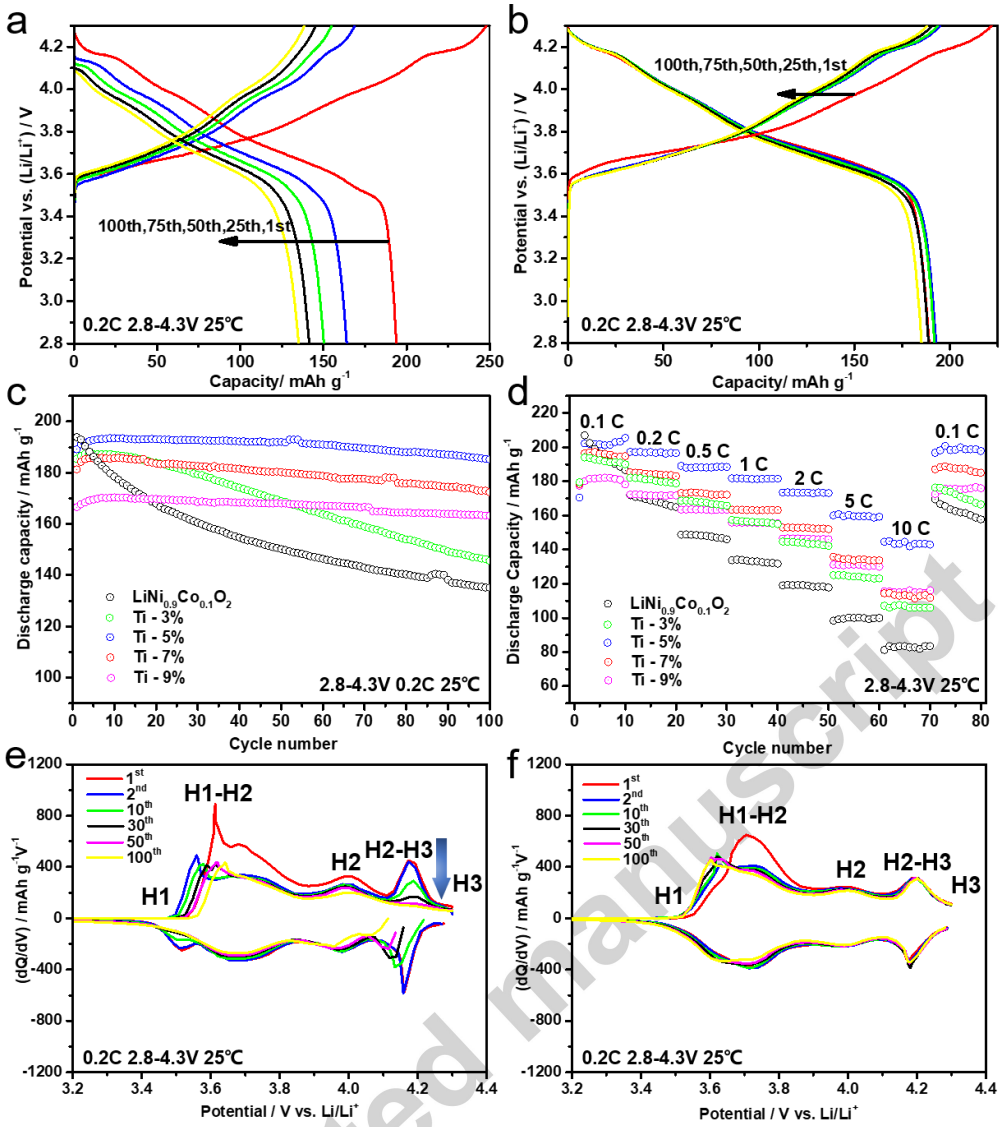

Fig. 3. Charge/discharge curves of (a) UM and (b) 5%-Ti PM at 0.2 C from 1st to 100th cycles. (c) Cycle performances of all the samples at 0.2 C within 100 cycles. (d) Rate capability of all the samples ranging from 0.1 C to 10 C. All the tests were applied within 2.8-4.3 V at 25 ℃ (1 C=190 mAh g^{-1}). (e, f) The corresponding differential capacity *vs.* voltage curves of Fig. 3a-b.

This claim was then validated in a more rigorous way, i.e. we tested the electrochemistry performances of the UM and 5%-Ti PM within 2.8-4.5 V voltage range and at 55 °C (Fig. S7). It is well-known that higher state-of-charge or elevated temperatures will lead to a more thorough delithiated state, making the layered structure more fragile. Surprisingly, even cycled in the voltage range of 2.8-4.5 V, the 5%-Ti PM sample displays 86.03% capacity retentions after 100 cycles at 0.2 C. In

contrast, the UM sample declines from 208.8 mA h g^{-1} to 124 mA h g^{-1} with a 59.39% capacity retention. The high-temperature test gave the similar results. Compared to the UM sample, the 100th capacity retention is significantly improved from 63.49% to 85.84% after Ti^{4+} doping. In line with results of Fig. 3, the dQ dV^{-1} profiles imply that the improved cycling performance and enhanced stability are related to the enhanced reversibility of H2-H3 phase transition (Fig. S7 c-d and g-h).

3.3 Mechanism analysis.

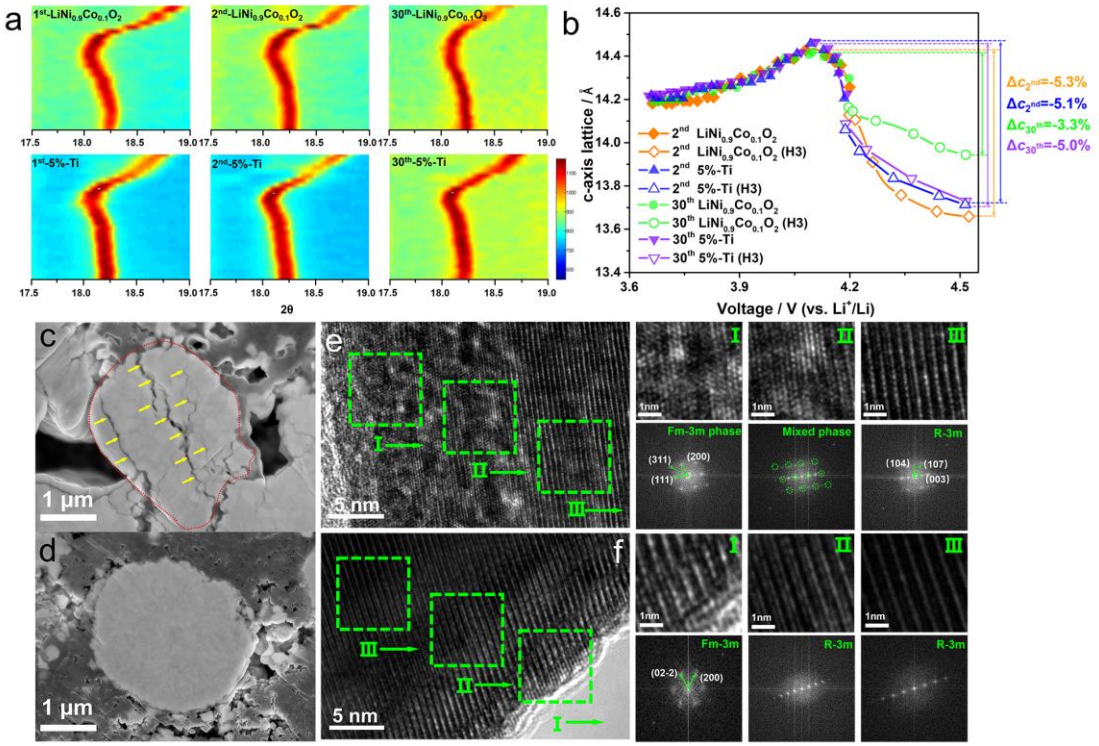

Fig. 4. (a) Contour plots of the in situ XRD patterns in 2θ range of the (003) reflection during the 1st, 2nd and 30th charge cycle for the UM and 5%-Ti PM; (b) c-axis lattice parameters as a function of the cell voltage for 2nd and 30th cycled UM and 5%-Ti PM. SEM images of the FIB-prepared cycled electrodes (0.5 C, 2.8-4.5 V after 30 cycles): (c) UM and (d) 5%-Ti PM. HRTEM images and the corresponding FTT images of cycled electrodes from the surface to the bulk (0.5 C, 2.8-4.5 V after 30 cycles): (e) UM and (f) 5%-Ti PM.

We then further conducted the in-situ XRD on the UM and 5%-Ti PM during the 1st, 2nd and 30th charging process, to express the *c*-axis lattice changes, and explore the phase evolution visually. As shown in Fig. 4a and Fig S8 a-f, in the second cycle, the (003) diffraction peaks of both samples shifted to lower diffraction angles when charging to ~4.1 V, and then shifted to higher 2θ values after charging to 4.2 V, indicating the formation of H2 and H3 phase respectively.[25] After 30 cycles, the H3 diffraction peaks of the UM sample became broadened in conjunction with decreased intensity, and almost disappeared after 50 cycles (Fig. S8 g-h); while, the H3 diffraction peaks of 5%-Ti PM showed unobservable changes, which is consistent with the lossless H3 oxidation peaks after long cycles shown in the dQ dV^{-1} plots (Fig. 3f). Hence, it can be confirmed that the preformed cation-mixing layer in 5%-Ti PM sample can keep its H3 phase intact in the extended cycles. Fig. 4b summarizes the lattice parameter *c* changes during the charging process shown in Fig. 4a. In the second cycle, there's an abrupt *c*-axis lattice parameter contraction in both UM (Δc=-5.3%) and 5%-Ti PM (Δc=-5.1%) samples after being charged above 4.1 V. After 30 cycles, the lattice parameter *c* change of the UM sample became dramatically reduced (Δc=-5.3%→-3.3%), while such a reduction is absent in the 5%-Ti PM sample (Δc=-5.1% → -5.0%). It's interesting that although the drastic lattice contraction has always existed within 30 cycles in the case of 5%-Ti PM sample, it exhibits superior cycling performance (Fig. 3c). This phenomenon may prompt us to reconsider the role of H3 phase, whose formation used to be considered as one of the origins for structure deterioration.[17, 26-28]

The main concern about H3 formation is that it might induce microcracks during cycling.[17] Surprisingly, Fig. 4d shows there are no microcracks being observed in the cycled 5%-Ti PM particles, displaying an obvious contrast to the microcracks marked by yellow arrows shown in Fig. 4c. This result implies that reversible H2-H3 phase transition makes the contraction in crystallographic *c*-direction reversible as well, thus the generation of microcracks can be suppressed. Further, we investigated the structures of cycled cathodes by HRTEM (Fig. 4e-f). Three different microregions from the surface to bulk are marked by Ⅰ, Ⅱ and Ⅲ. Fig. 4e shows the layered structure of the UM sample has been disrupted after high-voltage cycling, displaying a presence of *Fm*-$\bar{3}$*m* phase, mixed phases and *R*-$\bar{3}$*m* phase from region Ⅰ to Ⅲ. While for the 5%-Ti PM, no obvious structural degradation appeared in the most regions compared with the fresh material. The layered-spinel-rock salt structural transformations seemed to be terminated since the H2-H3 phase transition became reversible. Accordingly, the 5%-Ti PM exhibits a lower onset exothermic temperature with less heat generation than the UM sample (Fig. S9), indicating remarkably enhanced structural and thermal stability.

Based on the above results and analysis, it is conjectured that during the repeated charge-discharge process of Ni-rich cathode materials, the existence of H3 phase can be served as their property-indicator, which reflects the high capacity delivery as well as the highly delithiated state. Indeed, the emergence of abundant Li vacancies at highly delithiated state will leave the structure vulnerable, and further suffer from structural transformation and microcracks generation along with the loss of H3 phase,

just like the behaviors of the UM sample here. However, the formation of H3 phase should not be the prerequisite of such a material degradation. If we can improve the reversibility of H2-H3 phase transition, for example through reconstructing the Ni-rich material surface to form a cation-mixing layer in this work, the Ni-rich material will exhibit high capacity and superior structural stability simultaneously.

4. Conclusion

In summary, layered Ni-rich $LiNi_{0.9}Co_{0.1}O_2$ cathode material was successfully synthesized by coprecipitation method. This pristine material was then doped by different content of Ti^{4+}. XRD and HRTEM characterizations revealed that a surface nanoscale cation-mixed layer would be formed after Ti^{4+} doping. This preformed cation-mixed layer has been determined to make the H2-H3 phase transition reversible. The improved reversibility of the H2-H3 phase transitions can not only suppress the generation of microcracks and structural transformations, but also allow continuous high capacity delivery. Consequently, the Ti^{4+} doped sample with an optimal content of 5 mol% exhibited excellent cycling performance without sacrificing the capacity. The 100^{th} capacity retention at 0.2 C was improved remarkably from 69.7% to 97.9% after the doping. These results imply that the strategy of improving the reversibility of the H2-H3 phase transition is feasible to simultaneously realize high capacity and stable cyclability of Ni-rich cathode materials

Acknowledgements

This work was supported by National Key R&D Program of China (2016YFB0100301), National Natural Science Foundation of China (21573017, U1664255) and China Postdoctoral Science Foundation (2017M620636, 2018T110050).

Appendix A. Supporting information

Supplementary data associated with this article can be found in the online version at doi:.

References

[1] S.-T. Myung, F. Maglia, K.-J. Park, C.S. Yoon, P. Lamp, S.-J. Kim, Y.-K. Sun, ACS Energy Lett. 2 (2017) 196-223.

[2] J. Liu, J.-G. Zhang, Z. Yang, J. P. Lemmon, C. Imhoff, G. L. Graff, L. Li, J. Hu, C. Wang, J. Xiao, Adv. Funct. Mater. 23 (2013) 929–946.

[3] B. Xu, C.R. Fell, M. Chi, Y.S. Meng, Energy Environ. Sci. 4 (2011) 2223-2233.

[4] B. Dunn, H. Kamath, J.M. Tarascon, Science 334 (2011) 928-935.

[5] J.W. Fergus, J. Power Sources 195 (2010) 939-954.

[6] E. Antolini, Solid State Ion. 170 (2004) 159-171.

[7] A. Manthiram, J.C. Knight, S.-T. Myung, S.-M. Oh, Y.-K. Sun, Adv. Energy Mater. 6 (2016) 1501010.

[8] W. Liu, P. Oh, X. Liu, M.J. Lee, W. Cho, S. Chae, Y. Kim, J. Cho, Angew. Chem. Int. Ed. 54 (2015) 4440-4457.

[9] Y. Koyama, H. Arai, I. Tanaka, Y. Uchimoto, Z. Ogumi, Chem. Mater. 24 (2012) 3886-3894.

[10] H. Yu, Y. Qian, M. Otani, D. Tang, S. Guo, Y. Zhu, H. Zhou, Energy Environ. Sci. 7 (2014) 1068-1078.

[11] K. Kang, Y.S. Meng, J. Bréger, C.P. Grey, G. Ceder, Science 311 (2006) 977-980.

[12] J. Xu, F. Lin, M.M. Doeff, W. Tong, J. Mater. Chem. A 5 (2017) 874-901.

[13] U.-H. Kim, S.-T. Myung, C.S. Yoon, Y.-K. Sun, ACS Energy Lett. 2 (2017) 1848-1854.

[14] K. Zhu, T. Wu, Y. Zhu, X. Li, M. Li, R. Lu, J. Wang, X. Zhu, W. Yang, ACS Energy Lett. 2 (2017) 1654-1660.

[15] M.-H. Choi, C.S. Yoon, S.-T. Myung, B.-B. Lim, S. Komaba, Y.-K. Sun, J. Electrochem. Soc. 162 (2015) A2313-A2318.

[16] B.J. Hwang, Y.W. Tsai, C.H. Chen, R. Santhanam, J. Mater. Chem. 13 (2003) 1962-1968.

[17] C.S. Yoon, H.-H. Ryu, G.-T. Park, J.-H. Kim, K.-H. Kim, Y.-K. Sun, J. Mater. Chem. A 6 (2018) 4126-4132.

[18] D. Zeng, J. Cabana, J. Bréger, W.S. Yoon, C. P. Grey, Chem. Mater. 19 (2007) 6277-6289.

[19] S. Hwang, S.M. Kim, S.M. Bak, B.W. Cho, K.Y. Chung, J.Y. Lee, W. Chang, E.A. Stach, ACS Appl. Mater. Interfaces 6 (2014) 15140-15147.

[20] S. Hwang, S.M. Kim, S.M. Bak, K.Y. Chung, W. Chang, Chem. Mater. 27 (2015) 6044-6052.

[21] R. Robert, C. Bünzli, E.J. Berg, P. Novák, Chem. Mater. 27 (2015) 526-536.

[22] L. Wang, T. Maxisch, G. Ceder, Chem. Mater. 19 (2007) 543-552.

[23] J. Zheng, T. Liu, Z. Hu, Y. Wei, X. Song, Y. Ren, W. Wang, M. Rao, Y. Lin, Z. Chen, J. Am. Chem. Soc. 138 (2016) 13326-13334.

[24] S.M. Bak, K.W. Nam, W. Chang, X. Yu, E. Hu, S. Hwang, E. A. Stach, K.B. Kim, K.Y. Chung, X.Q. Yang, Chem. Mater. 25 (2013) 337-351.

[25] J. Xu, E. Hu, D. Nordlund, A. Mehta, S. N. Ehrlich, X. Yang, W. Tong, ACS Appl. Mater. Interfaces 8 (2016) 31677-31683.

[26] J. Yang, Y. Xia, ACS Appl. Mater. Interfaces 8 (2016) 1297-1308.

[27] H.J. Noh, S. Youn, C.S. Yoon, Y.-K. Sun, J. Power Sources 233 (2013) 121-130.

[28] C.S. Yoon, D.W. Jun, S.T. Myung, Y.-K. Sun, ACS Energy Lett. 2 (2017) 1150-1155.

[29] Y. Cho, P. Oh, J. Cho, Nano Lett. 13 (2013) 1145-1152.

[30] J. Zhao, W. Zhang, A. Huq, S. T. Misture, B. Zhang, S. Guo, L. Wu, Y. Zhu, Z. Chen, K. Amine, Adv. Energy Mater. 7 (2017) 1601266.

[31] J. Yang, Y. Xia, J. Electrochem. Soc. 163 (2016) A2665-A2672.

[32] J.-N. Zhang, Q. Li, Y. Wang, J. Zheng, X. Yu, H. Li, Energy Storage Mater., 14 (2018) 1-7.

[33] J. Li, W. Li, Y. You, A. Manthiram, Adv. Energy Mater., 8 (2018) 1801957.

[34] L. Zou, Z. Liu, W. Zhao, H. Jia, J. Zheng, Y. Yang, G. Wang, J.-G. Zhang, C. Wang, Chem. Mater., 30 (2018) 7016-7026.

[35] B. Xiao, X. Sun, Adv. Energy Mater., 8 (2018) 1802057.

Vitae

Feng Wu is the director of the Green Energy Research Institute, and the vice president of the China Battery Industry Association. As the chief scientist, he has hosted the National Key Program for Basic Research of China (973 projects), Basic Research on New Rechargeable Batteries and Related Materials. He has published over 500 papers and has been awarded 45 patents. In 2012, he was awarded the IBA Research Award for outstanding research of battery material and systems for electric vehicles. In 2017, Prof. Wu was elected as an academician of the Chinese Academy of Engineering.

Na Liu is currently a Ph.D. candidate under supervision of Prof. Feng Wu in the School of Materials Science and Engineering at Beijing Institute of Technology. Her research is focus on the design, synthesis, performance improvement and structural characterization of Ni-rich cathode materials for high performance Lithium ion batteries.

Lai Chen obtained his Ph.D. majoring in Environmental Engineering from Beijing Institute of Technology (BIT) in 2017, and is currently a postdoctoral fellow at the school of Materials Science and Engineering at BIT. As the principal investigator, he has successfully hosted the National Natural Science Foundation of China and China Postdoctoral Science Foundation. His research interests focus on synthesis chemistry, nano science and developing high-energy cathode materials for LIBs.

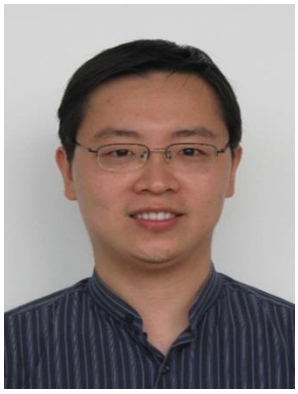

Yuefeng Su is a professor in the School of Materials Science and Engineering at Beijing Institute of Technology (BIT). In 2013, he was awarded New Century Excellent Talents in University from the Chinese Ministry of Education. His research group mainly engaged in the research of green secondary batteries and advanced energy materials, including lithium-rich cathode materials, nickel-rich cathode materials and other high-power energy storage devices. As the principal investigator, Prof. Su successfully hosted the National Key Research and National Natural Science Foundation of China, etc.

Guoqiang Tan received his Bachelor degree in 2007 from Hunan University, and his Ph.D. degree in 2014 from Beijing Institute of Technology under the supervision of Prof. Feng Wu, China. He is currently a postdoctoral fellow at Chemical Sciences and Engineering, Argonne National Laboratory, USA. His research interests focus on advanced materials and battery configurations for high energy rechargeable battery systems.

Liying Bao is currently a professor in the School of Materials Science and Engineering at Beijing Institute of Technology (BIT). She received her Ph.D. degree from BIT in 2007. As the principal investigator, Prof. Bao successfully hosted the National Natural Science Foundation of China. Her research focuses on electrochemical energy storage and conversion technology.

Qiyu Zhang is currently a Ph.D. candidate under supervision of Prof. Yuefeng Su in the School of Materials Science and Engineering at Beijing Institute of Technology. He received his B.S. degree from Beijing Jiaotong University in 2016. His research focuses on the performance improvement and structural optimization of Ni-rich cathode materials for high-performance Lithium ion batteries.

Yun Lu is currently an instructor in School of Material Science & Engineering, Beijing

Institute of Technology (BIT). She received her B.E. in Polymer Materials from BIT in 2001, and Ph.D. in Materials Science and Engineering from BIT in 2006. Her research majors in Polymer-based electrolytes for Li-S battery and aerogels of conductive polymers. Dr. Lu has published more than 10 articles in the field of Energy Storage up to now.

Jing Wang is currently an associate professor in the School of Materials Science and Engineering at Beijing Institute of Technology (BIT). She was a visiting scholar in University of Georgia for one year. She received her Ph.D. degree from BIT in 2003. She participated in the national 863 major electric vehicle special project and 973 major basic research development planning project research work. Her research focuses on the high capacity anode materials and high power battery testing technologies.

Shi Chen is a professor in the School of Materials Science and Engineering at Beijing Institute of Technology (BIT). He has been working at BIT since 1986. As the principal investigator, Prof. Shi Chen successfully hosted the National High Tech. 863 project, National Natural Science Foundation. His research interests are low cost electrode materials for lithium ion batteries.

Jing Tan is an associate professor in the School of Chemistry and Chemical Engineering at Beijing Institute of Technology. She received her Ph.D. degree from Tsinghua University in 2011 and completed her postdoctoral appointee from Tsinghua University in 2014. Her major research is focus on the microchemical technology to optimize the chemical process.

Highlights

- A surface nanoscaled cation-mixing layer is fabricated for Ni-rich material through appropriate surficial Ti^{4+} substitution.
- This preformed cation-mixing layer can improve the reversibility of H2-H3 phase transition.
- Reversible H2-H3 phase transition contributes to realize both high capacity and stable cyclability for the Ni-rich cathodes.